Thermal Analysis for a High Precision Pointing Helios CubeSat

A Project Presented to
The Faculty of Aerospace Engineering
San José State University

In Partial Fulfillment of the Requirements for the Degree
Master of Science in Aerospace Engineering

by

Justin E. Lai

December 2015

The Designated Project Committee Approves the Project Titled

THERMAL ANALYSIS FOR A HIGH PRECISION POINTING
HELIOS CUBESAT

by

Justin E. Lai

ABSTRACT

THERMAL ANALYSIS FOR A HIGH PRECISION POINTING HELIOS CUBESAT

by Justin Lai

The thermal control subsystem (TCS) maintains the temperature of the Helios CubeSat to be within the allowable operational and survival temperature limits. Due to the limited size and weight of a CubeSat, a passive TCS was chosen. This report used two analytical models to determine the CubeSat temperature resulting from environmental heating: 1) a steady state model and 2) a transient model. For each model temperatures were determined for a CubeSat with no thermal control and with various thermal coatings. The resulting temperatures were then compared to typical temperature limits for on-board components to determine if they could survive and operate through the course of the specified mission.

Two cases were investigated under the steady state model: a hot case and a cold case. The hot case with no thermal control yielded a temperature of 41.6 °C, while the cold case with no thermal control yielded a temperature of -98.9 °C. The transient model offered a different temperature range from 92.0 °C at its highest to -24.3 °C at its lowest. Although the results were different between the two models, the transient model yielded better results than the steady state model when compared to typical temperature limits for on-board components.

Table of Contents

List of Figures

List of Tables

Nomenclature

A = Area
A_{al} = Area of aluminum surface
A_{lat} = Area of CubeSat lateral face
A_{long} = Area of CubeSat longitudinal face
A_s = Area of solar cell surface
a = Semi-major axis
c_p = Specific heat capacity
e = Eccentricity
F_{12} = View factor
F_a = Albedo view factor
F_e = Eclipse function
f_e = Eclipse fraction
G = Universal gravitational constant, 6.67×10^{-11} m^3/kgs^2
H = Altitude
i = Inclination
M = Mass (for Earth, 5.972×10^{24} kg)
m = Mass of spacecraft
P = Orbital Period
P_e = Period in eclipse
Q_a = Steady state heat absorbed
Q_A = Steady state heat absorbed from albedo
Q_E = Steady state heat absorbed from Earth infrared
Q_e = Steady state heat emitted
Q_S = Steady state heat absorbed from direct solar radiation
Q_S' = Transient heat absorbed from direct solar radiation
R_e = Radius of the Earth
r_a = Radius at apogee
r_p = Radius at perigee
S = Heat flux of solar radiation
S' = Heat flux from albedo
S_E = Heat flux from Earth infrared
T = Temperature
t = Time

α = Absorptivity
α' = Weighted average of absorptivity
α_{al} = Absorptivity of Aluminum 6061-T6
α_{lat} = Absorptivity of lateral face
α_{long} = Absorptivity of longitudinal face
α_s = Absorptivity of GaAs solar cell
β = Beta angle
δ_s = Declination of the Sun
ε = Emissivity
ε' = Weighted average of emissivity

ε_{al} = Emissivity of Aluminum 6061-T6

ε_s = Emissivity of GaAs solar cell

θ = Angle of incidence between surface and incident radiation

θ_{lat} = Angle of incidence on lateral face

θ_{long} = Angle of incidence on longitudinal face

σ = Stefann-Boltzmann constant

ν = True anomaly

ϕ = Orbit angle

ϕ_{es} = Angle at which eclipse begins

ϕ_{ee} = Angle at which eclipse ends

ω = Argument of perigee

Ω = Right ascension of the ascending node

Ω_s = Right ascension of the Su

1.0 Introduction

1.1 Motivation and Objectives

Coronal mass ejections (CME) are bursts of magnetized plasma ejected from the Sun's corona formed from magnetic flux ropes, plasma joined together by their magnetic field lines[1]. CMEs can travel through interplanetary space from 100 km/s to 3000 km/s. At the higher range of speeds, they can disturb the steady flow of solar wind and create a shock wave, which further energizes any particles in the solar wind[2]. This energized flow of particles eventually impacts the Earth's magnetic field resulting in geomagnetic storms.

As the energized particles reach the Earth, energy in the form of heat is added to the Earth's ionosphere, increasing the density of Earth's upper atmosphere[3]. The higher density increases the drag on satellites in low-earth orbit (LEO), affecting their operation. Geomagnetic storms can also induce geomagnetic currents in the power grid and create errors in navigation systems like GPS or the Global Navigation Satellite System[3]. Astronauts aboard the International Space Station must use caution so that they are not exposed to the increased radiation. The strength of geomagnetic storms depends on the direction of the magnetic field of the CME. If the magnetic field of the CME is opposite that of the Earth's magnetic field, the storms tend to be large[3].

Predicting the strength of CMEs and when they will impact the Earth is essential because of the effect CMEs have on the Earth. The National Aeronautics and Space Administration (NASA) in 2014 had an annual operating budget for missions related to heliophysics of $68M with an investment of $5.5B in 18 operating missions and 29 spacecraft[4]. Recently, efforts have been made to reduce the cost of space exploration through the use of small satellites called CubeSats.

The CubeSat was first developed through a joint effort between California Polytechnic State University, San Luis Obispo (Cal Poly) and the Space Systems Development Laboratory (SSDL) at Stanford University. Since then numerous universities have designed and developed CubeSats as a hands-on educational tool for undergraduate and graduate students. A standard 1 kg, 10 cm by 10 cm by 10 cm cube shaped spacecraft is a one unit (1U) CubeSat. Standard size CubeSats can be joined together to form 2U, 3U, or 6U CubeSats. The standardized buses of CubeSats mean they require less time to build and are thus more cost effective than large-scale satellites, particularly for institutions with limited budgets and workforce.

Under the guidance of NASA Ames Research Center, a partnership was formed by San Jose State University (SJSU) and the University of Idaho to develop the Technology-Educational Satellite (TechEdSat). The TechEdSat has shown that valuable science can be obtained from nanosatellites and be a stepping-stone toward larger satellites.

Currently there are many readymade attitude determination and control systems (ADCS) available for CubeSats. However, they are high in cost and offer very little flight heritage. In an effort to reduce cost, a project has been proposed to design, develop, and test an ADCS for a CubeSat that will accurately point at the Sun. Under the leadership of NASA Ames Researcher, Dr. Nagi Mansour, and SJSU Professor, Dr. Periklis Papadopoulos, SJSU graduate and undergraduate students will design and develop a high precision pointing Helios CubeSat.

1.2 CubeSat Subsystems

A CubeSat typically consists of a few important subsystems that control attitude determination and control, communication, power, command and data handling, and thermal control. The attitude determination and control subsystem (ADCS) controls the stabilization of

the spacecraft and orients it in the desired direction. Without ADCS a satellite will rotate

aimlessly through space, but because instruments are typically directed toward certain objects,

the attitude must be controlled. Common attitude control systems include spin stabilization,

dual-spin stabilization, three-axis spin stabilization, and gravity gradient[5]. Gravity gradient

controlled spacecraft are perhaps the most passively controlled. They are the least expensive, but

have the lowest pointing accuracy[5]. Spin-stabilized spacecraft are passively controlled and are

low cost, but they are inefficiently powered and have low pointing accuracy. Dual spin

spacecraft are more complex than spin-stabilized spacecraft, which adds to the cost, but they

have pointing capabilities and propellant control. Spacecraft stabilized in three axes are the most

expensive, heaviest, and complex, but they give the highest pointing accuracy. The mission

objectives, requirements of the other subsystems, cost, and weight determine which ADCS is

required for a spacecraft.

The communications subsystem is responsible establishing communication for tracking,

gathering data on the other systems, and transmitting that data back to Earth. The

communications subsystem may also be responsible for responding to autonomous commands

and failure situations.

The command and data handling subsystem (C&DH) is responsible for command –

receiving and distributing commands to the other subsystems – and telemetry – gathering and

transmitting mission data. The design of the C&DH depends on the size and design of the

spacecraft, but the C&DH can be divided into three categories: single unit, multi-unit, and

integrated unit. The single unit C&DH has one unit for command and one unit for telemetry. A

multi-unit C&DH system uses a remote unit that is physically removed from the spacecraft to

distribute commands and handle data. An integrated C&DH system integrates command,

telemetry, and attitude control into one system. This last system helps reduce cost and the amount of required hardware because all of its functions are handled in one unit.

The electrical power system (EPS) provides and distributes the spacecraft electrical power. Without a power source the other subsystems and the payload could not function properly. There are four common types of power sources: photovoltaic, static, dynamic, and fuel cells[6]. Photovoltaic solar cells convert solar radiation to electrical energy and are usually used on spacecraft orbiting the Earth. A static power source uses a heat source and converts it to electrical energy using a nuclear reactor. A dynamic power source performs the same function as a static power source, but through the use of a Brayton, Stirling, or Rankine cycle[6]. Fuel cells are often used in manned space missions.

The thermal control subsystem (TCS) is responsible for regulating the temperature of a spacecraft such that it falls within to thermal limits: survival temperature limits and operational temperature limits[6]. The survival temperature limits are the limits the spacecraft must be in at all times even when the on-board instruments are not operating. These limits exist because of environmental heating, radiation from the environment that heats the spacecraft, and the fact that materials used to construct a spacecraft can only survive within a certain range of temperatures. Therefore, a TCS ensures that a spacecraft can withstand heat generated by its environment.

 The operational temperature limits are the limits the instruments must be in while they are operating. Unlike the environment, which constantly heats the spacecraft, the instruments typically expel heat only when they are operating. However, the instruments can only operate successfully if they operate within a certain range of temperatures. For example, batteries typically operate between 5 and 20°C[6]. Therefore the TCS must maintain the batteries'

temperature to be within 5 and 20°C. The success of a mission depends on the temperature of the spacecraft not exceeding its survival and operational limits[6].

The project presented in this report focuses on designing and evaluating a passive TCS based on TechEdSat heritage for the Helios CubeSat. The TCS will ensure that the internal and external temperatures of the CubeSat do not exceed or fall below the thermal limits imposed by the design of the CubeSat.

1.3   Methods of Thermal Control

The surface temperature of the Earth is regulated in part by Earth's atmosphere and albedo. By reflecting and absorbing some sunlight, these mechanisms act as Earth's thermal control subsystem (TCS), which make Earth habitable for life. A spacecraft in space is void of such mechanisms unless a TCS is part of the design of the spacecraft.

The TCS of a satellite can be active, passive, or a combination of the two. An active TCS is typically more complex in design and higher in cost and weight. However, an active TCS is useful in satellites that have components that dissipate large amounts of heat. A passive thermal control subsystem is typically used on small satellites such as the CubeSat because it is lighter, more power efficient, and least expensive[7]. Passive TCS are also considered more reliable than active TCS. As a result spacecraft are initially designed with passive thermal controls and with active controls added as needed.   Considering the Helios CubeSat is limited in size and weight, a passive TCS will be used and be the area of interest for this project.

One method to passively control the temperature of a spacecraft is through the use of a thermal coating, for example, paint. White and black paint are used most often because of their emissivity and absorptivity abilities. Emissivity is the ratio of emitted energy by a nonblack

surface to the emitted energy if it were a blackbody at the same temperature[8]. A blackbody has an emissivity of one since it is a perfect emitter. It emits all incident radiation that it absorbs. However, a spacecraft is not a blackbody. Incident radiation is absorbed, reflected, or transmitted into the body of the spacecraft. Absorptivity is the percentage of incident radiation that is absorbed by the spacecraft. When choosing a thermal coating, it is necessary to consider the emissivity and absorptivity of the coating to ensure proper temperature control.

A disadvantage to thermal coatings is degradation. Objects in space are bombarded by charged particles and ultraviolet radiation[9]. For an object in LEO, the leading cause of surface coating degradation is atomic oxygen (AO)[9]. UV radiation from the Sun causes molecular oxygen, O_2, in the Earth's upper atmosphere to break apart into atomic oxygen, or individual atoms of oxygen. This process is known as photodissociation. Surface coating degradation typically increases solar absorptivity while having little effect on its infrared emittance. The increase in solar absorptivity presents a problem when designing a thermal control system because a TCS is designed to handle a certain load of thermal radiation.

Another method to passively control the thermal environment is through the use of multi-layered insulation (MLI). MLI blankets keep the internal components of a spacecraft sufficiently warm while preventing excessive heating from the environment[9]. A typical MLI blanket consists of layers of Mylar or Kapton that are less than 1 mm thick. Each side of the layers has a gold or aluminum reflective coating. For a spacecraft in LEO, an MLI blanket typically has 15-20 reflective layers[10]. A cross section schematic of an MLI blanket is shown in Figure 1[10].

Heat transfers through an MLI blanket by radiation, solid conduction, and gaseous conduction[9]. Each form of heat transfer is minimized differently. For example, using as many reflective layers as necessary to properly insulate the spacecraft can minimize radiative heat

transfer. Adding spacers as shown in Figure 1 helps reduce contact between layers, which will reduce the amount of solid conduction.

MLI blankets have been used extensively on many successful missions. This is in part due to guidelines established by NASA on material selection, design, and assembly[10]. The outer layer shown in Figure 1 acts as a protective cover for the reflective layers from corrosion in space, particularly from the effects of atomic oxygen. To prevent erosion from atomic oxygen, materials must be shielded from or made with material resistant to atomic oxygen[10]. According to NASA the outer material must also be resistant to "shedding, flaking, and other forms of particulate generation." If the outer material is not opaque to UV radiation, then the reflective layer must be directly under the outer layer. Reflective layers are typically perforated to avoid "ballooning" during ascent[10]. Table 1 shows examples of MLI blankets and their developers[11].

Typical Multilayer Insulation Stacking Arrangement
(Section of book in parentheses)

Outer Cover (4.1.1)
Light Block (If necessary)
Metallized Reflector (4.1.2)
Netting Spacer (4.1.3)

Exposed Threads (4.2.2)   Adhesive Transfer Tape (4.4.1)   Glass Fabric Tape (4.4.2)
Nonexposed Threads (4.2.1)   Metallized Tape (4.4.3)
(15 to 20 Reflector/Spacer Layers, Total)   Adhesives (4.3)   Grounding Tape (4.4.4)
Hook-and-Pile
Connectors (4.5.1)

Metallized Seflector (4.1.2)
Netting Spacer (4.1.3)
Inner Cover (4.1.4)
Structure

Note: Details and features are shown for illustration and will vary with actual design and installation.

Figure 1: Cross section schematic of an MLI blanket[10].

Table 1: Examples of MLI Blankets[11]

Technology	Description	Company	TRL Status	Figure
MLI blanket	Materials include polyimide films, Nome threads, and PTFE impregnated glass cloth	Aerospace, Fabrication and Materials, (USA)	9 Sucessfully used on SCISAT I and ISS*	
MLI blanket	Aluminized polyester, polymide, or flurocarbon	Dunmore (USA)	9 Sucessfully flown on CASSINI/HUYGENS PROBE, ISS, and FUSE*	
MLI blanket	Aluminized (one/two sided) polyester, or polymide	SHELDAHL (USA)	9 Sucessfully applied on BIRD	

The TRL status in Table 1 refers to the Technology Readiness Level standard for measuring the readiness of a particular technology[12]. There are nine levels with TRL 1 being the lowest and TRL 9 being the highest. A piece of technology receives a rating after it's been evaluated against a set of parameters that define each level. The MLI blankets shown in Table 1 all have TRL 9, which means they have been "flight proven" and have been successfully used on multiple missions. A technology is rated TRL 9 after it's been successfully used on a mission.

In theory, an MLI blanket should be impenetrable to radiation. The reflective layers on a blanket have a low emissivity, and if these layers are stacked upon each other, the blanket should be near impenetrable to radiation. This works in theory. However, due to imperfections, edge and fin effects, and bending and molding of the blanket to accommodate the surfaces of the spacecraft, an MLI blanket is not completely resistant to radiation[8]. Therefore, the performance of an MLI blanket is measured by its effective emittance[6]. An MLI blanket is most effective with a low effective emissivity. Larger spacecraft will have a lower effective emittance than

smaller spacecraft. Figure 2 can be used to estimate the performance of an MLI blanket using

aluminized Mylar layers. It should be noted that adding more insulation layers than is required

does not improve the performance of the MLI blanket. There is a point at which the radiative

heat transfer between layers becomes so small that it renders layers beyond this point practically

useless[9].
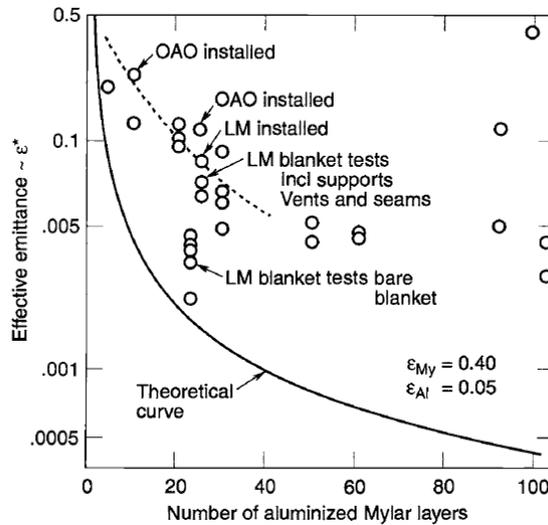
Figure 2: Relationship between the number of MLI layers and its effective emittance[9].

A common device used to transport heat dissipated by electrical devices into space is a

heat pipe as shown in Figure 3[13]. In a typical heat pipe, there is a layer of liquid and a layer of

vapor. When one end of the pipe is heated, the liquid absorbs the heat and evaporates. As the

liquid evaporates, a pressure difference is established between the two ends of the pipe. The

difference in pressure forces the vapor to flow towards the cooler end of the pipe, where the

vapor condenses into liquid, expelling heat in the process. The liquid then flows back to end it

originated and the cycle continues.
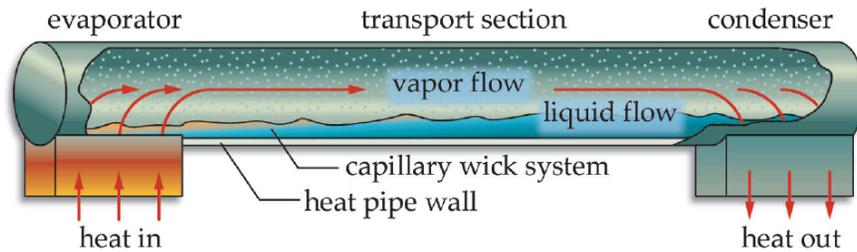
Figure 3: Schematic of a heat pipe[13].

A relatively new technology has been developed for passive TCS called variable emittance coating (VEC). The advantages of having VEC is that the emissivity can vary depending on circumstances unlike paint or MLI blankets, which have a constant emissivity. The idea behind VEC is to provide space missions that may experience large variations in power usage or environment with a low cost method of thermal control[14].

When choosing the method of thermal control, the type of ADCS used on the spacecraft can be a factor because different attitude control methods result in different exposures to the Sun. For example, the surfaces of a spin-stabilized satellite alternate between being exposed to the Sun and being in shadow for short cycles, typically with a spin rate of 60 to 90 rev/min[15]. Conversely, a surface on a three-axis stabilized satellite can be exposed to the Sun for a very long period. The result is a much more complex TCS design.

1.4 Thermal Control in Previous and Current Missions

In 2001 Shin *et al*. analyzed the transient temperature of the Korea Multi-Purpose Satellite (KOMPSAT) solar array to show how the temperature of the solar array varied during its orbit[16]. Figure 4 shows the time evolution of the array's temperature, or transient temperature of the array. The method to model the transient temperature will be discussed in Section 2.3. The moments the solar array would be in eclipse is clearly indicated by the large decrease in

temperature. At approximately 67 minutes into the array's orbit, there is a large increase in temperature, which indicates the moment the array begins to transit back into sunlight. It should be noted that although the KOMPSAT orbited the Earth in LEO, it was also in a sun-synchronous orbit. If an object is said to orbit the same position from the perspective of the Sun, then the object is in a sun-synchronous orbit.
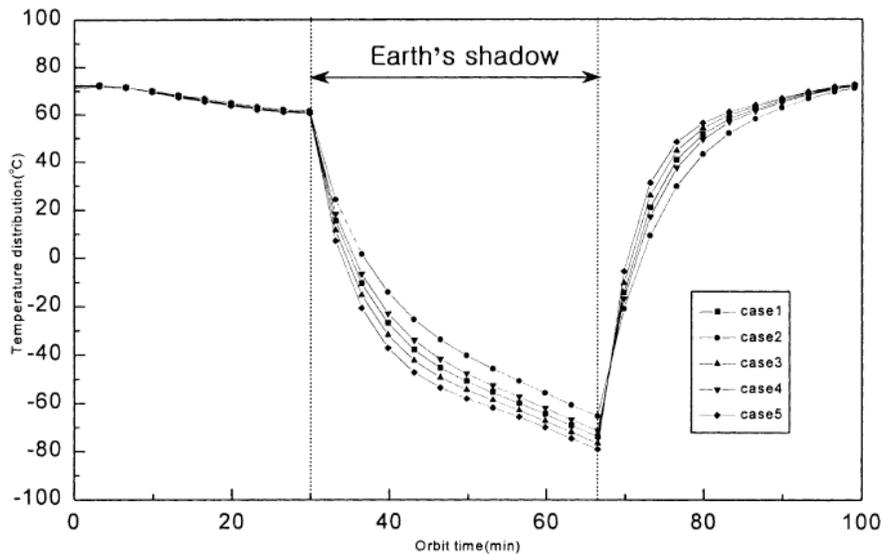
Figure 4: Time evolution of the temperature of the KOMPSAT solar array[16].

In 2001 HAMSAT, a micro-satellite used to provide satellite services for amateur radio, used a completely passive TCS for simplicity and reliability[17]. Orbiting in a sun-synchronous orbit, the 42.5 kg CubeSat consisted of a 0.73 kg TCS. Body mounted gallium arsenide (GaAs) solar cells and a lithium battery supplied the power to HAMSAT. Since the solar cells covered the four longitudinal faces, the two lateral faces were the only faces that could directly radiate heat back to space. Heat was radiated out of a 280mm x 280mm "window" created by white paint on the bottom face of the satellite. The degradation of the white paint was not a concern because it was never exposed to direct sunlight. The remaining area of the bottom face was

covered with 15 layers of MLI. Other surfaces also used 15 layers of MLI and low emittance tape.

Like KOMPSAT, Narayana and Reddy modeled the temperature of HAMSAT using a transient temperature model, which will be discussed in detail in Section 2.3. Figure 5 compares the predicted time evolution of the temperature with on-board measurements. The predicted temperature and the measured temperature closely match, which validates the transient temperature model used by Narayana and Reddy. Therefore, this model will be used to predict the transient temperature of the Helios CubeSat.
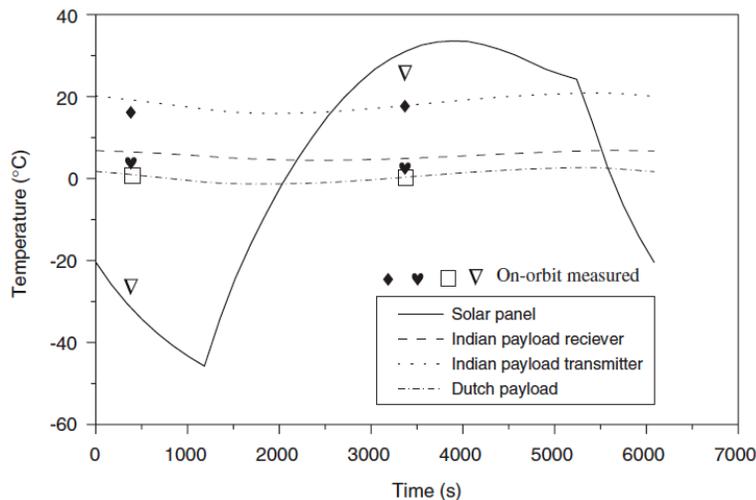
Figure 5: Comparison of predicted HAMSAT temperature with measured temperature[17].

The University of Colorado Boulder is currently developing a 3U CubeSat called The Miniature X-Ray Solar Spectrometer (MinXSS). Currently scheduled for launch at the end of 2015, MinXSS uses a passive TCS to radiate energy from the spacecraft to space[18]. The outer surfaces not facing the Sun are covered with aluminum Kapton tape to radiate energy. These radiators operate at a temperature ranging from -28°C to -11°C. Temperature is actively controlled on the batteries and the onboard spectrometer. The batteries use a thermal heater,

while the X123 detector head, which must be kept at -50°C ± 20°C, uses a Thermal Electric Cooler (TEC)[18].

There have been four successful TechEdSat missions. The first TES (TechEdSat) was jettisoned from the International Space Station (ISS) on October 4, 2012. It successfully operated for seven months before re-entering the Earth's atmosphere. This was followed by another successful mission by TES-2, which launched on August 21, 2013. On November 19, 2013, the first 3U CubeSat, TES-3, was successfully launched from the ISS and successfully demonstrated a new de-orbit technique using an Exo-Brake system. TES-4 was jettisoned from the ISS in March of 2015 to demonstrate a passive deorbiting system to reenter Earth's atmosphere[19]. Of the 4 TES missions, none have shown any issues regarding thermal control. The Helios CubeSat will follow TES-2, -3, and -4 in using a TCS that began with TES-1.

In 2006 three micro-satellites, Space Technology 5 (ST5), were launched to validate new technologies[20]. Part of its mission was to be a proof-of-concept for VECs. The VECs were not integrated into ST5's passive TCS but were "stand alone" experiments and separate from the overall system. The VEC radiator consisted of a composite metalized polymer, which allowed for radiative and conductive heat transfer. This allowed the surface of the satellites to vary emissivity. The validation of the VEC encountered some problems and requires further development.

2.0 The Space Environment

2.1 Radiation

There are three mechanisms of heat transfer: conduction, convection, and radiation. Heat transferred by conduction occurs when the molecules of a warm object collide with the molecules of a cool object. The molecules in the warm object have more kinetic energy than the molecules in the cool object, and thus, the warm molecules move faster. When the molecules collide, some of the energy from the fast molecules is transferred to the slow molecules in the form of heat. Convection is the transfer of heat through motion of a fluid. When liquids or gases are heated, they become less dense and begin to move towards cooler areas. Cooler liquids or gases replace the areas once occupied by the warm liquids or gases, and the process repeats itself. Radiation is heat transfer by electromagnetic waves. No contact between objects and no medium is required for heat to transfer via radiation. This is the primary mean of heating of a spacecraft as introduced in the previous section and is the scope of this project.

The Helios CubeSat will be designed to point at the Sun with high precision while in low-earth orbit (LEO), where it will be exposed to direct solar radiation, sunlight reflected off the Earth (albedo), and infrared energy emitted by the Earth as shown in Figure 6[12]. The Sun being the closest and brightest object in the solar system is the greatest source of thermal radiation. At 1 AU, the average intensity of solar radiation is approximately 1358 W/m^2. The albedo of the Earth varies with the land, ocean, cloud cover, and latitude[9]. While the amount of sunlight and albedo a spacecraft is exposed to depend on its orbit, a spacecraft will always be exposed to the Earth's infrared radiation. Earth's infrared radiation, sometimes known as outgoing longwave radiation (OLR), is the sunlight that was absorbed by the Earth and reemitted. These three forms

of radiation contribute to environmental heating. It is the responsibility of the TCS to ensure a spacecraft can survive the temperatures resulting from environmental heating.
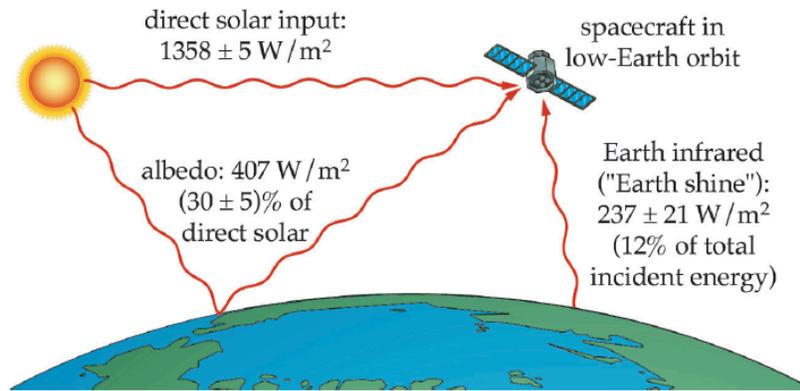
Figure 6: Satellite thermal environment[12].

2.2   Steady State Environmental Thermal Analysis

A preliminary step in designing a TCS for a spacecraft is to quantify and determine the amount of environmental heating. As stated previously, there are three forms of environmental heating as shown in Figure 4: direct solar heating, Q_S, Earth albedo heating, Q_A, and Earth infrared heating, Q_E. The heat resulting from direct solar radiation and Earth albedo radiation are dependent on the incident angle of the radiation to the surface of the spacecraft, the surface's area and absorptivity, and the intensity of the radiation.

$$Q_S = S\alpha A \cos\theta \qquad (2.2.1)$$

$$Q_A = S'\alpha A \cos\theta \qquad (2.2.2)$$

where

$$S' = \text{albedo of planet} \times S \qquad (2.2.3)$$

The heat resulting from Earth's infrared is dependent on the intensity of the radiation, surface's area and emissivity, and a view factor.

$$Q_E = A\epsilon F_{12}S_E \qquad (2.2.4)$$

It should be noted that the emissivity of the satellite's surface is used in Equation (2.2.4) instead of the absorptivity because the energy being emitted by the Earth is infrared. S in Equations (2.2.1-4) is dependent on the source of radiation, while the area, absorptivity, and emissivity are properties of the surface of the spacecraft. The angle θ is the angle the radiation makes with respect to the normal of the surface.

Since Earth is not a point source of radiation in relation to a spacecraft in LEO, only a fraction of the energy emitted by the Earth is radiated onto the surface of the spacecraft[21]. The view factor, F_{12}, in Equation (2.2.4) is the fraction of thermal energy leaving an isothermal surface that directly hits another surface. It depends on the geometry of the two surfaces.

$$F_{12} = \left(\frac{1}{A_1}\right) \int_{A_1} \int_{A_2} \left(\frac{\cos\beta_1 \cos\beta_2}{\pi r_{12}^2}\right) dA_1 dA_2 \qquad (2.2.5)$$

where β_1 and β_2 are the angles that the normal of areas dA_1 and dA_2, respectively, make with distance r_{12} between them (see Figure 7)[22].
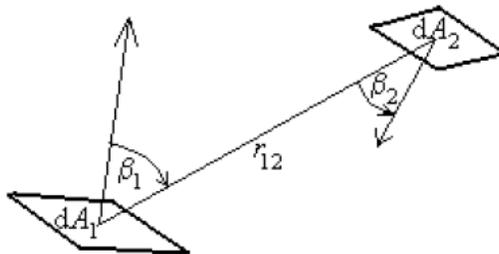
Figure 7: View factor geometry[21].

The CubeSat also radiates heat into space. According to the Stefan-Boltzmann law, all surfaces above absolute zero emit radiation that is proportional to their temperature to the fourth power:

$$Q_e = \epsilon A \sigma T^4 \qquad (2.2.6)$$

16

where $\sigma = 5.66 \times 10^{-8}$ W/m^{2}K.

An energy balance is used to determine the temperature of the CubeSat.

$$\frac{dE}{dt} = Q_a - Q_e \tag{2.2.7}$$

where

$$Q_a = Q_S + Q_A + Q_E \tag{2.2.8}$$

Since a steady state is being considered, energy will not vary with time, so the left hand side of the energy balance equals zero. Rearranging Equation (2.2.7) such that the absorbed heat equals the emitted heat yields an expression for the temperature of the CubeSat.

$$Q_a = Q_e \tag{2.2.9}$$

$$S\alpha A \cos\theta + S'\alpha A \cos\theta + A\epsilon F_{12}S_E = \epsilon A\sigma T^4 \tag{2.2.10}$$

$$T = \left(\frac{S\alpha A \cos\theta + S'\alpha A \cos\theta + A\epsilon F_{12}S_E}{\epsilon A\sigma}\right)^{\frac{1}{4}} \tag{2.2.11}$$

Two cases are usually explored when calculating the temperature of a spacecraft: a hot case and a cold case. The hot case analyzes the hottest temperature a spacecraft might reach. This typically occurs when the spacecraft receives the most amount of thermal energy such as when the spacecraft is in direct sunlight. In contrast, the cold case analyzes the lowest temperature a spacecraft might reach. This typically occurs when the spacecraft receives the least amount of thermal energy such as when the spacecraft is in eclipse.

2.3 Transient Environmental Thermal Analysis

While the temperature calculated by Equation (2.2.10) provides a foundation for the thermal analysis of a spacecraft, it does not provide an accurate representation of what occurs thermally to a spacecraft while in orbit. Equation (2.2.10) calculates the temperature at a specific point and assumes the satellite is stationary at that point. In reality, the satellite's temperature

will not instantaneously reach the hot or cold case temperature while transiting from direct sunlight to eclipse or vice versa. Therefore, an analysis to study how the temperature evolves while the spacecraft is in orbit must be performed.

The transient thermal analysis uses the same equations used in Section 2.2 with a few modifications. The solar energy absorbed by the satellite is still calculated by Equation (2.2.1). However, for a time history of the energy absorbed, a step function is used[23].

$$Q_S' = S\alpha A F_e \qquad F_e = \begin{cases} 0 & \text{if } \phi_{es} < \phi < \phi_{ee} \\ 1 & \text{otherwise} \end{cases} \qquad (2.3.1)$$

where if the angle along an orbit is known, then ϕ_{es} and ϕ_{ee} are the angles in radians where eclipse begins and ends, respectively.

If a circular orbit is assumed, the angles at which eclipse begins and ends are found by

$$\phi_{es} = \pi - \arccos\left(\frac{\sqrt{h^2 - 1}}{h\cos\beta}\right) \qquad (2.3.2)$$

$$\phi_{ee} = \pi + \arccos\left(\frac{\sqrt{h^2 - 1}}{h\cos\beta}\right) \qquad (2.3.3)$$

where h is a function of relative orbit radius

$$h = \frac{H + R}{R} \qquad (2.3.4)$$

The time at which ϕ_{es} and ϕ_{ee} occur can be determined by

$$\frac{t}{P} = \frac{\phi}{2\pi} \qquad (2.3.5)$$

A modification must also be made to Equation (2.2.2), which calculates the heat input as a result of albedo. The direction sunlight is reflected off a planet changes as the spacecraft orbits the planet. To account for this, the cosine term in Equation (2.2.2) is put in terms of the beta angle and orbit angle[23]. The necessary modification depends on the altitude of the spacecraft. For simplicity, altitudes will be grouped into two categories: high and low orbits. Altitudes less than 320 km will be considered low orbits[23].

For low orbits the cosine term in Equation (2.2.2) is modified by using the law of spherical cosines, where

$$\cos\theta = \cos\phi\cos\beta \qquad (2.3.6)$$

Thus, the heat absorbed from albedo is

$$Q_A{}' = S'\alpha A F_a \qquad (2.3.7)$$

where F_a is known as an albedo view factor and is defined as[23]

$$F_a = \cos\phi\cos\beta F_e \qquad F_e = \begin{cases} 1 & \text{if } -\frac{\pi}{2} < \phi < \frac{\pi}{2} \\ 0 & \text{otherwise} \end{cases} \qquad (2.3.8)$$

For high orbits, the albedo view factor is given by

$$F_a = \left(\frac{1+\cos\phi}{2}\right)^2\left[1 - \left(\frac{\phi}{\phi_{es}}\right)^2\right]\cos\beta\, F_e \qquad F_e = \begin{cases} 0 & \text{if } -\phi_{es} < \phi < \phi_{es} \\ 1 & \text{otherwise} \end{cases} \qquad (2.3.9)$$

Similar to the steady state case, an energy balance is used to calculate the temperature of the CubeSat, where the heat absorbed uses the modified solar and albedo heat fluxes.

$$\frac{dE}{dt} = Q_S' + Q_A' + Q_E - Q_e \qquad (2.3.10)$$

If $dE = mc_p dT$ is substituted into Equation (2.3.10), a first order ordinary differential equation is obtained[23].

$$mc_p\frac{dT}{dt} = S\alpha A F_e + S'\alpha A F_a + A\epsilon F_{12}S_E - \epsilon A\sigma T^4 \qquad (2.3.11)$$

It should be noted that for the analysis presented here it is helpful to express dT/dt as $dT/d\phi$, since F_e and F_a are functions of ϕ. dT/dt can be converted to $dT/d\phi$ using the relationship expressed by Equation (2.3.5). An Euler or Runge-Kutta method can be used to solve Equation (2.3.11), which will yield the transient temperature of a spacecraft. If the temperature is plotted against time, then the time history of the temperature can be shown.

2.4   Orbital Mechanics

When analyzing the thermal environment of a spacecraft, certain orbital elements must first be determined including how long the spacecraft will be exposed to the radiations previously described. The first relevant orbital element is eccentricity, *e*. Orbits are one of four conic sections; they are circular, elliptical, parabolic, or hyperbolic (see Figure 8)[6]. An orbit's eccentricity determines the type of conic section. An eccentricity of zero means the orbit is circular. An eccentricity greater than zero but less than one means the orbit is elliptical. An eccentricity equal to one is a parabola, and greater than one results in a hyperbolic orbit.
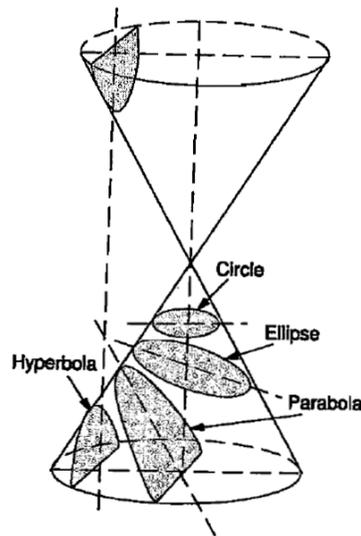
Figure 8: Conic sections used to define orbits[6].

Another parameter that describes an orbit is inclination, *i*. An object orbiting the Earth is typically described with respect to the equatorial plane of the Earth, the plane of the Earth's equator[9]. The angle at which the orbital plane is away from the equatorial plane of Earth is the orbit's inclination.   While inclinations greater than 98° are possible, most orbits have

inclinations between 0 and 98°. Satellites with inclinations greater than 98° have a retrograde orbit, or orbit the Earth opposite of Earth's rotation[9].

If an orbit is circular or elliptical, it will cross Earth's equatorial plane at two locations: the ascending node and descending node. The ascending node is the point on the orbit at which the spacecraft crosses the equatorial plane while moving south to north. Likewise, the descending node is the point at which the spacecraft crosses the equatorial plane while moving from north to south, or descending.

The altitude of the satellite also plays an important role in analyzing the satellite's thermal environment as will be discussed later. The altitude of a spacecraft is the distance the spacecraft is above Earth's surface, while the highest and lowest altitudes are known as apogee and perigee, respectively. The average of the orbit's radius at apogee, r_a, and radius at perigee, r_p, is the semi-major axis, a.

$$a = \frac{r_a + r_p}{2} \tag{2.4.1}$$

Eccentricity is related to the radii of perigee and apogee and the semi-major axis by

$$r_p = a(1 - e) \tag{2.4.2}$$

$$r_a = a(1 + e) \tag{2.4.3}$$

If the semi-major axis of the orbit is known, then orbit's period can be determined.

$$P = 2\pi \sqrt{\frac{a^3}{GM}} \tag{2.4.4}$$

The above parameters describe an object's position in an elliptical orbit using a geocentric-equatorial coordinate system (see Figure 9)[6]. An object's position is sometimes described using the celestial coordinate system (see Figure 10)[9]. The celestial coordinate system is an extension of Earth's equator to an infinite radius and forming a fictitious, celestial sphere[9]. Two important angles used to describe an object's position are right ascension and declination.

Right ascension is an angle in the equatorial plane and is measured from the vernal equinox. Therefore, the right ascension of ascending node, Ω, is the angle of the ascending node measured from the vernal equinox. The angle describing the position of an object above or below the equatorial plane is declination.
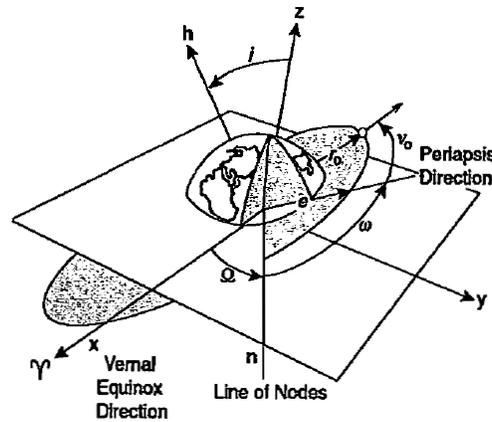
Figure 9: Orbital parameters in a geocentric-equatorial coordinate system[6].
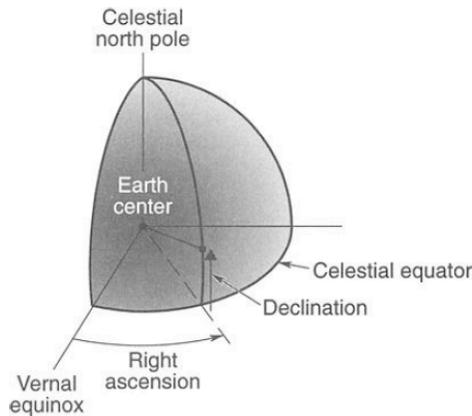
Figure 10: Right ascension and declination in the celestial coordinate system[9].

Two more angles worth mentioning are the argument of perigee and true anomaly. The argument of perigee, ω, is the angle measured from the ascending node to the orbit's perigee in the direction of the object's motion. The true anomaly, v, is the angle between the orbit's perigee and the position of the satellite and is measured in the satellite's direction of motion.

A final orbital element relevant to analyzing the thermal environment of a satellite is its beta angle. The beta angle is defined as the angle between the orbital plane of the satellite and the solar vector as shown in Figure 11[9]. The beta angle is used to determine the amount of time a satellite will be eclipsed by the object the satellite is orbiting. Since the Helios CubeSat will not be stationary as it points at the Sun, there will be instances where the Earth will eclipse the CubeSat. While in eclipse, the spacecraft will not be exposed to any solar or albedo radiation. Therefore, it is essential to determine the amount of time the spacecraft will spend in eclipse.

Mathematically, the beta angle is defined by Equation (2.4.5) and can vary from -90 to 90 degrees[9]. It should be noted that the angle β in Figure 11 and Equation (2.4.5) is not the same as the angle β in Figure 7 and Equation (2.2.5).

$$\beta = \sin^{-1}(\cos \delta_s \sin i \sin(\Omega - \Omega_s) + \sin \delta_s \cos i) \tag{2.4.5}$$
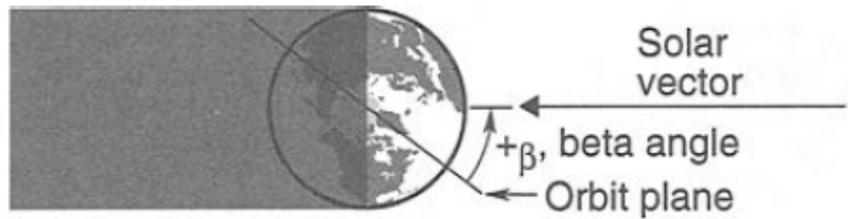
Figure 11: Illustrative representation of an orbit's beta angle[9].

The time a spacecraft spends in eclipse varies with β. As can be inferred from Figure 11, an orbit with β equal to 0 will have the longest eclipse time because it is shadowed by the full diameter of the Earth. As β increases, eclipse times decrease until β equals 90 degrees, where eclipse time equals zero. A quantitative relationship between eclipse time and beta angle is described by Equation (2.4.6), which gives the fractional time a satellite spends in eclipse for a circular orbit[7].

$$f_e = \frac{1}{180°} \cos^{-1} \left[\frac{(h^2 + 2R_e H)^{\frac{1}{2}}}{(R_e + H) \cos \beta} \right] \tag{2.4.6}$$

Therefore, if the period a satellite is known, then the amount of time a satellite spends in eclipse is

$$P_e = P f_e \tag{2.4.7}$$

Equation (2.4.6) was evaluated in MATLAB for altitudes, h, of 200, 400, 600, and 800 km, and an Earth radius, R_e, of 6371 km. The beta angle varied from a range of 0 to 90 degrees. This yielded an eclipse fraction for each altitude at each beta angle. Table 2 presents some of the results from the calculations. A graphical representation of the results is shown in Figure 12.

Table 2: Eclipse Fraction for Select Altitudes

Beta Angle [deg]	Altitude [km]			
	200	400	600	800
0	0.421	0.390	0.367	0.348
10	0.420	0.388	0.365	0.346
20	0.416	0.383	0.358	0.338
30	0.409	0.372	0.345	0.322
40	0.396	0.354	0.322	0.296
50	0.376	0.323	0.282	0.247
60	0.337	0.263	0.199	0.130
70	0.246	0.045	0	0
80	0	0	0	0
90	0	0	0	0

Table 2 and Figure 12 show that an object will spend less time in eclipse as the beta angle and altitude increases. Likewise, a spacecraft with a low altitude and low beta angle will spend more time in direct sunlight. Table 2 and Figure 12 also show that for each altitude there is a beta angle at which point the satellite will not experience any eclipse and will remain in direct sunlight through its entire orbit.
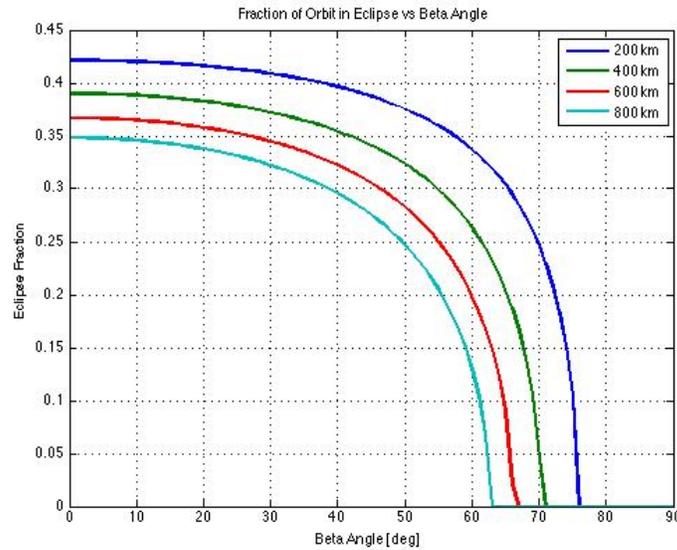
Figure 12: Relationship between eclipse fraction and beta angle.

The effect an orbit's beta angle has on the amount of time a satellite spends in eclipse is demonstrated further in Figure 13 by plotting and maintaining known orbital parameters while varying the beta angle. Figure 13 was plotted in MATLAB using the orbital parameters of the International Space Station (ISS) (see Table 3). MATLAB code used to plot Figure 13 can be seen in Appendix A. For the purposes of this demonstration, it was assumed that the orbit's inclination angle and the orbit's beta angle are equal. However, this is not the case in reality because the orbital plane of the ISS is not parallel to Earth's equatorial plane. For an orbit's inclination and beta angles to be equal, the orbital plane and Earth's equatorial plane must be parallel.

Table 3: Known Orbital Parameters of the International Space Station

Orbital Parameter	
Right Ascension of Ascending Node [deg]	290.4
Argument of perigee [deg]	331.3
True Anomaly [deg]	189.8
Semi-Major Axis [km]	6784.5
Eccentricity	0.0005
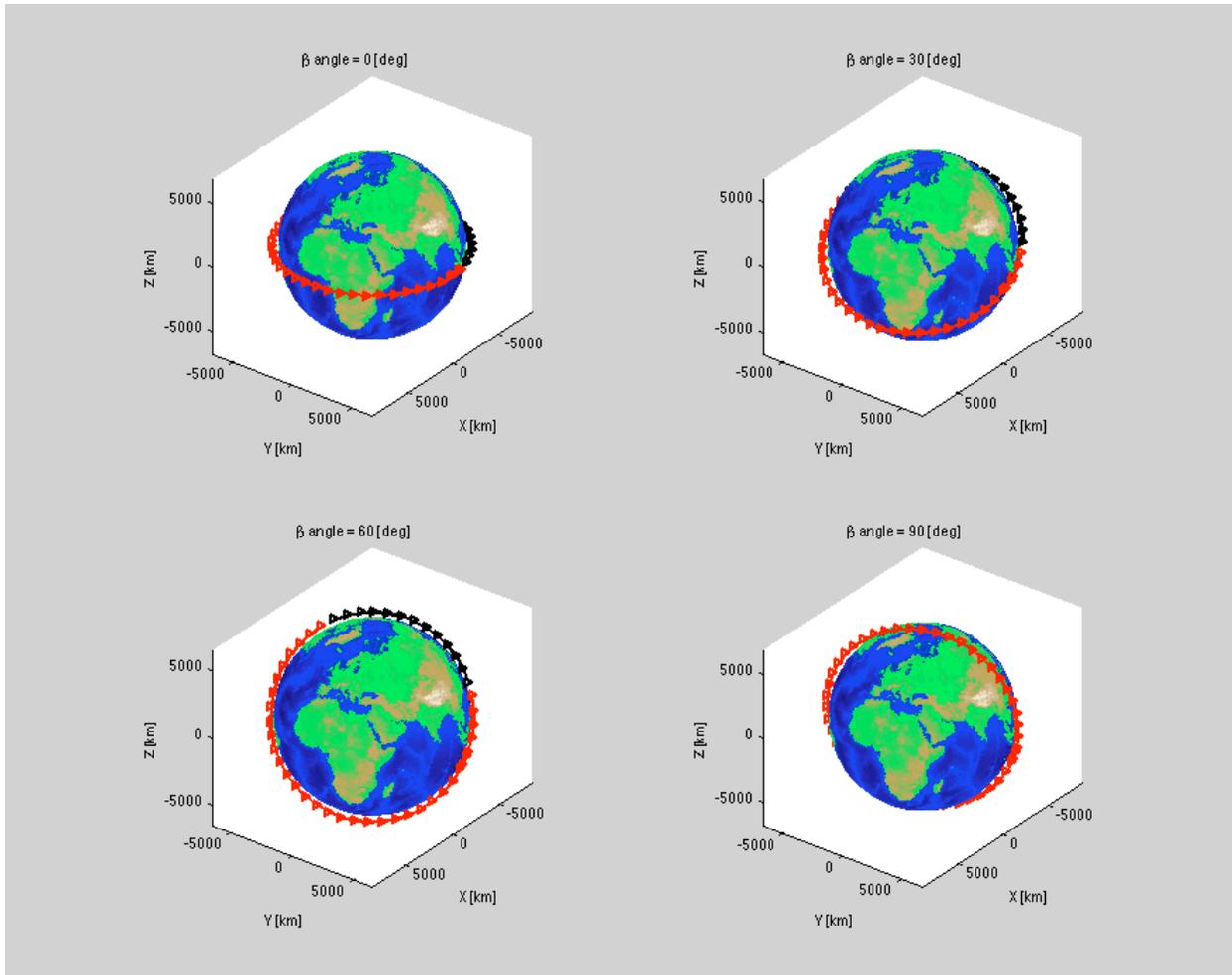
Figure 13: Variations in eclipse time with varying beta angles.

The plots in Figure 13 show how beta angle affects eclipse time. All of the orbital parameters in Table 3 were held constant. Inclination was the only parameter that was modified to simulate the effects of different beta angles, which, recall, for the purposes here inclination is assumed to equal beta angle. If it is also assumed the solar vector is penetrating the y-z plane, the red portion of the orbits would indicate when a spacecraft is in direct sunlight, while the black portion would indicate when a spacecraft is eclipsed by the Earth. Figure 13 further confirms that as the beta angle increases eclipse time decreases.

3.0 Steady State Thermal Analysis for Helios CubeSat

To obtain a general idea of the level of heating the Helios CubeSat will experience, the temperature of the CubeSat is determined first without the use of a TCS. Then, a thermal analysis is performed using a method of thermal control, specifically thermal coatings and finishes. Two cases will be examined to obtain temperature limits that CubeSat will experience: a hot case and a cold case. The hot case represents the time the CubeSat is in direct sunlight and will provide an upper temperature limit, while the cold case will give a lower temperature limit and represents the time the CubeSat is in eclipse. Knowing these two extreme temperatures is important because it can then be inferred that the temperature of the CubeSat at any point in its orbit will be between these two extremes.

3.1 Helios CubeSat Mission Profile

The Helios CubeSat is proposed to be a 3U CubeSat. Attached to one side of the CubeSat will be two solar panels each with a 3U area. In addition, body mounted solar cells will be mounted to the longitudinal sides of the spacecraft to act as a redundant system. The mounted solar cells will also be 3U in area except for the side with the deployable solar panels, which when deployed will be facing the Sun. The solar cells on that side will be 2U in area. A 1U area will be left exposed so that the on-board sun sensor will have an unobstructed view of the Sun.

The solar cells are proposed to be 29% NeXt Triple Junction (XTJ) solar cells. The absorptivity and emissivity of the solar cells are 0.9 and 0.85, respectively[24]. The structure of the CubeSat is proposed to consist of Aluminum 6061-T6, which has an absorptivity and emissivity of 0.379 and 0.0393, respectively[6]. A preliminary mockup created in AutoCAD of the CubeSat is shown in Figure 14 with its deployable solar panels in a collapsed position.
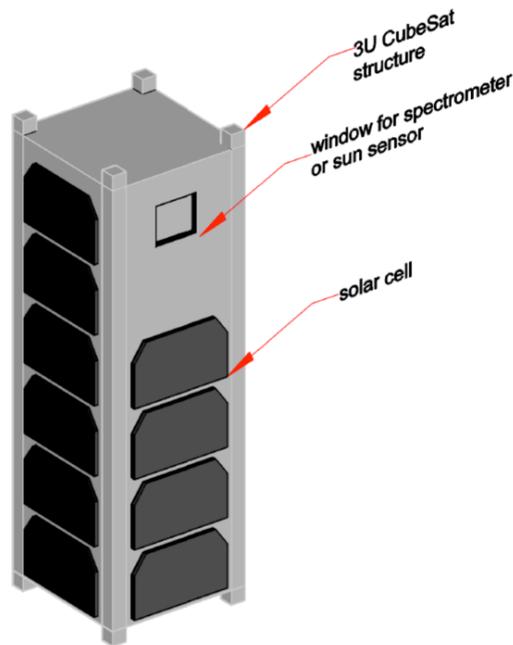
Figure 14: Preliminary design of Helios CubeSat (solar cells not to scale).

It is proposed that the CubeSat will be launched from the International Space Station (ISS). Specifics about the orbit of the CubeSat have yet to be determined, so for the purpose of the analysis presented in this report, it is assumed the CubeSat will have the same orbital parameters as the ISS. The CubeSat will have an altitude of 400 km, inclination of 51.6°, and orbital period of approximately 90 minutes. Using the same MATLAB code used to plot Figure 13, Figure 15 shows the trajectory for the Helios CubeSat. The orbit's beta angle is again assumed to be the same as the orbit's inclination. The portion of the orbit in red indicates when the CubeSat is exposed to direct sunlight, while the portion in black indicates when the Earth eclipses the CubeSat.
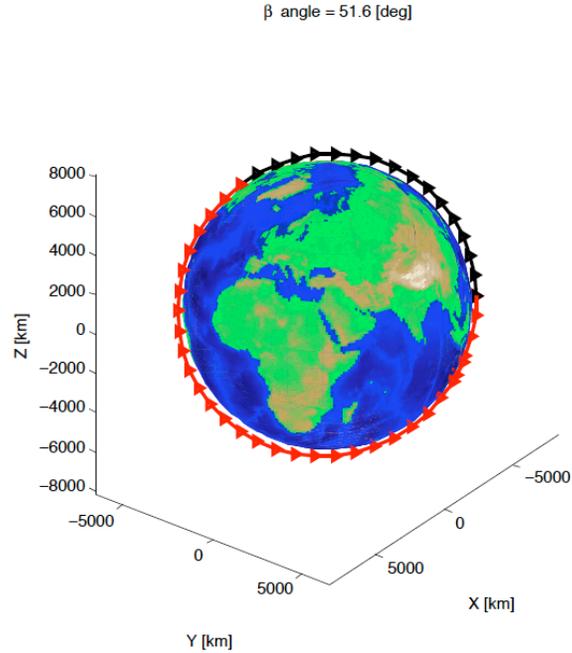
Figure 15: Trajectory of CubeSat following ISS orbit.

3.2 Hot Case and Cold Case with No TCS

To simplify the analysis, the following assumptions are made. It is assumed that three faces of the CubeSat are illuminated by the Sun: one longitudinal (30 cm x 10 cm) face and two lateral (10 cm x 10 cm) faces. In addition, sunlight is incident on the longitudinal face at 90°, while sunlight is incident on the lateral faces at 45°. Albedo and infrared radiation are assumed to be incident on one longitudinal face, the side facing the Earth, at 90° (see Figure 16). Lastly, it is assumed that all of the faces of the CubeSat are isothermal.

The view factor in Equation (2.2.5) can be approximated with[22]

$$F_{12} = \left(\frac{R_e}{R_e + H} \right)^2 \tag{3.2.1}$$

where R_e = 6371 km and H = 400 km.

29
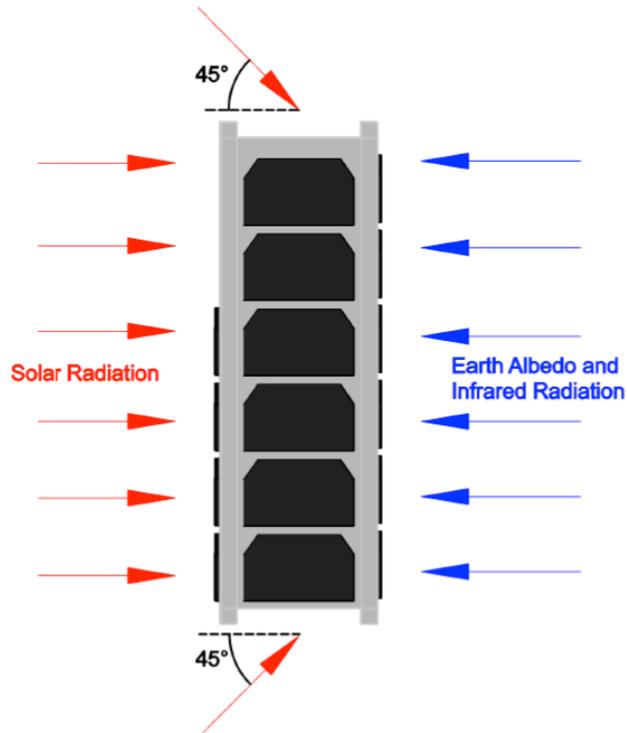
Figure 16: Angles of incidence of radiation on CubeSat.

From the *Spacecraft Thermal Control Handbook* the solar irradiation, Earth infrared, and albedo at an orbit assumed for the CubeSat is 1367 W/m², 257 W/m², and 0.26, respectively. Using these values, the assumptions above, and the energy balance described by Equation (2.1.7), the temperature of the CubeSat can be determined. For detailed calculations for the hot case temperature, see Appendix A. The CubeSat temperature obtained for the hot case is approximately 41.6°C.

The difference between the hot and cold cases is that there is zero solar radiation and albedo radiation in the cold case. From the *Spacecraft Thermal Control Handbook*, the heat flux from Earth infrared is 218 W/m². Like the hot case, the infrared radiation is incident on one longitudinal face at 90°. In addition, every surface of the CubeSat is assumed to be isothermal. The calculations for the cold case as shown in Appendix A yielded a temperature of -98.9 °C.

The calculated temperatures give the survival temperature limits as discussed in Section

1.2. For a CubeSat with no TCS, the temperatures would fluctuate between 41.6°C and -98.9 °C.

Table 4 gives some typical temperature limits for various spacecraft components[6]. When the hot

and cold case temperatures are compared to the operational and survival temperatures for the

components in Table 4, it can be seen that except for the solar panels, the CubeSat will be too

cold for the components when the spacecraft is in eclipse. It can also be seen that the reaction

wheels and C&DH box baseplates can survive and operate during the hot case, while the

batteries will neither operate nor survive. The only components that can survive both cases are

the solar panels.

Table 4: Typical Temperature Limits of Various Spacecraft Components.

Component	Typical Temperature Ranges [°C]	
	Operational	Survival
Batteries	0 to 15	-10 to 25
Reaction Wheels	-10 to 40	-20 to 50
C&DH Box Baseplates	-20 to 60	-40 to 75
Solar Panels	-150 to 110	-200 to 130

3.3   Hot Case and Cold Case with Thermal Finishes

Similar calculations as those performed in the previous section are performed with

different coatings and finishes. The same CubeSat design, solar cells, and assumptions used in

the previous section are used here. However, instead of using the absorptivity and emissivity of

the CubeSat's aluminum structure, the absorptivities and emissivities of a few common thermal

surface finishes as shown in Table 5 are used[9]. As discussed in Section 1.3 surface coatings

degrade over the life span of a mission. Therefore, the absorptivities presented in Table 5 are the

values at the start of the mission. Table 6 shows the calculated hot and cold case temperatures

for the surface coatings presented in Table 5. For the coatings that have a range of absorptivities,

the average was used to calculate the surface temperature.

Table 5: Absorptivity and Emissivity of Common Thermal Surface Coatings[9]

Surface Coating	Absorptivity α	Emissivity ε
Optical Solar Reflector		
2-mil silvered Teflon	0.05 to 0.09	0.66
2-mil aluminized Teflon	0.10 to 0.16	0.66
White Paint		
PCBZ	0.16 to 0.24	0.87
Black Paint		
3M Black Velvet	0.97	0.84
Aluminized Kapton		
2 mil	0.41	0.75
Metallic		
Vapor-deposited gold	0.19 to 0.30	0.03
FSS-99 (overcoated silver)	0.03	0.02

Table 6: Temperature of CubeSat with Surface Coating

Surface Coating	Hot Case [°C]	Cold Case [°C]
Optical Solar Reflector		
2-mil silvered Teflon	12.0	-106.6
2-mil aluminized Teflon	15.3	-106.6
White Paint		
PCBZ	14.5	-109.1
Black Paint		
3M Black Velvet	48.8	-108.5
Aluminized Kapton		
2 mil	27.5	-107.5
Metallic		
Vapor-deposited gold	35.0	-98.8
FSS-99 (overcoated silver)	23.2	-98.6
No coating	41.6	-98.9

When the hot and cold case temperatures of the CubeSat with a surface coating is compared with the temperatures in the no coating scenario, it can be seen that there is a decrease in the hot case temperature. This demonstrates that the surface coatings will help control the temperature when exposed to direct sunlight. When the hot case temperatures in Table 6 are compared with the temperature limits in Table 4, it can be seen that the components are more likely to survive the operational and survival limits than with no coating.

However, the coatings decreased the temperatures even further than if the CubeSat had no coating. This indicates that the CubeSat is losing a substantial amount of heat when it moves into eclipse and that a thermal control system must be designed to retain the heat that is accumulated when the CubeSat is in direct sunlight. This can be done with an MLI blanket. An MLI blanket will not only limit the amount of external thermal radiation from entering the CubeSat, but will also limit the amount of internal thermal radiation from leaving the CubeSat, which will potentially keep the internal components within their required temperature limits.

4.0 Transient Thermal Analysis for Helios CubeSat

The temperatures calculated in Section 3 predict the temperature bounds the CubeSat would experience. Therefore, the CubeSat at any point along its orbit is expected to have a temperature that is within those bounds. By following the process outlined in Section 2.3 and solving Equation (2.3.11) will show how the temperature evolves within the temperature limits calculated in the previous section, and yield the exact temperatures at any point along the orbit.

For the transient thermal analysis the same mission profile as that in Section 3 is assumed. In addition, the trajectory of the CubeSat is assumed to be as shown in Figure 17, where the orbital angle, ϕ, increases as the CubeSat orbits Earth in a counter-clockwise

direction[23]. It should be noted that where ϕ equals zero is the hot case as discussed in the previous section.
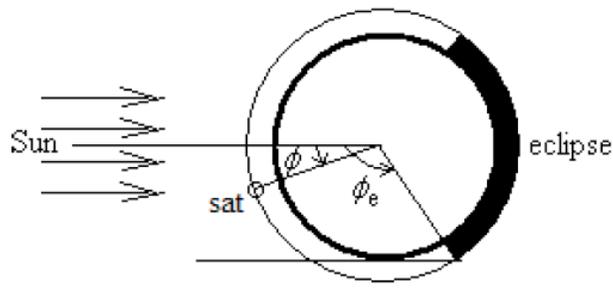
Figure 17: Defined trajectory and orbital angle direction for CubeSat[23].

Using Equations (2.3.2-3) the angles at which eclipse starts and ends are 123° (t = 30.9 min) and 237° (t = 59.5 min), respectively. Figure 18 shows the time evolution of the heat absorbed from solar radiation as calculated by Equation (2.3.1). While the CubeSat is exposed to direct sunlight, it receives 30 watts of energy, while in eclipse it receives zero.
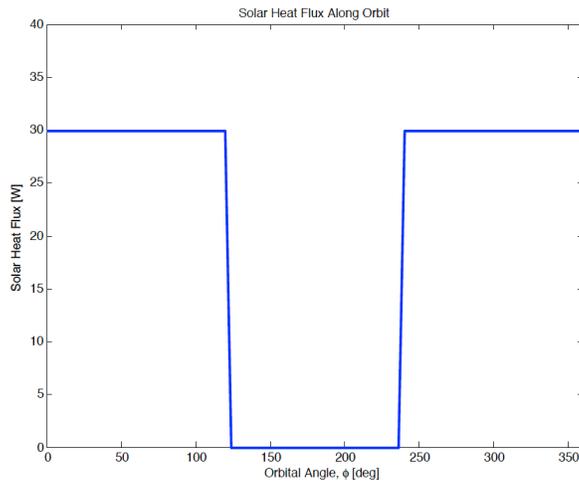
Figure 18: Time evolution of absorbed solar radiation along CubeSat orbit.

The heat absorbed resulting from albedo was calculated using Equation (2.3.7). Since the CubeSat is at an altitude of 400 km, the orbit is considered a high orbit, so Equation (2.3.9) was used to calculate the albedo view factor. Figure 19 shows the time history of the absorbed albedo radiation.
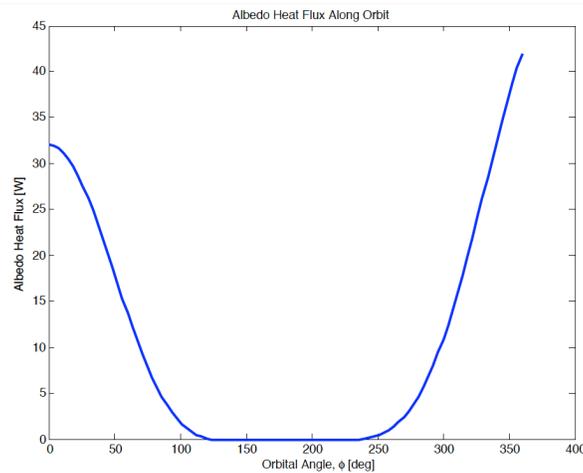
Figure 19: Time evolution of absorbed albedo radiation along CubeSat orbit.

The angles at which the albedo radiation equals zero are the angles at which the CubeSat is in eclipse. The fact that the radiation is zero means there is zero sunlight being reflected off of the Earth at those angles in the satellite's orbit.

Section 2.3 suggests using either an Euler or Runge-Kutta method to solve differential equation in Equation (2.3.11). However, an alternative method was used. An iterative process was used in MATLAB to calculate the temperature of the CubeSat at various points along its orbit (see Appendix C). First, an initial temperature was assumed. In this case, the hot case temperature of 41.6 °C, which was calculated in Section 3.2, was assumed. This initial temperature was substituted into the temperature term on the right hand side of Equation (2.3.11), and the differential $dT/d\phi$ was calculated. The differential $dT/d\phi$ indicated how much the temperature changed from one angle to the next. This change in temperature was then added

to the initial temperature, which yielded a new temperature. This process was repeated with the new temperature acting as the initial temperature.

For example, if the temperature at $\phi = 0$ was 41.6 °C, then by substituting T = 41.6 °C into Equation (2.3.11), $dT/d\phi$ equaled 10.8. This meant the temperature of the CubeSat increased by 10.8°C when the CubeSat transited from an orbital angle of 0 to 3.75°, resulting in a new temperature of 52.4 °C. This new temperature was substituted back into Equation (2.3.11), $dT/d\phi$ was recalculated, and a new temperature was given. The process continued for one complete orbit.

This analysis was first performed for a CubeSat with no thermal control mechanism. Table 7 presents selected data from the temperature calculations, and Figure 20 shows the time evolution of the temperature along the orbit of the CubeSat.

Table 7: Select Data of Transient Temperature

Initial Angle [deg]	Initial Temperature [°C]	$dT/d\phi$	Final Angle [deg]	Final Temperature [°C]
0	41.6	10.80	3.75	52.4
30	81.2	0.15	33.75	81.4
60	73.2	-1.82	63.75	71.4
90	58.4	-1.64	93.75	56.8
120	48.3	-0.74	123.75	47.6
150	3.4	-3.23	153.75	0.2
180	-14.0	-1.25	183.75	-15.2
210	-21.1	-0.55	213.75	-21.7
240	-24.3	9.34	243.75	-15.0
270	28.0	3.63	273.75	31.6
300	50.1	2.36	303.75	52.5
330	70.6	2.80	333.75	72.8
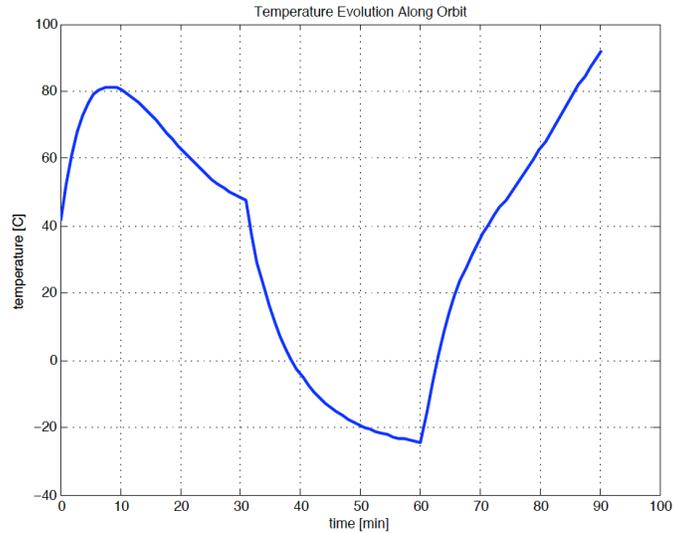
Figure 20: Time evolution of CubeSat temperature.

The temperatures calculated in Section 3.2 predict the upper and lower temperature limits of the CubeSat and the temperature at any point along the orbit of the CubeSat would exist somewhere between those limits. However, as Figure 20 shows, the maximum and minimum values of the transient temperature do not agree with the temperatures calculated using the steady state model. In fact, Figure 20 indicates the CubeSat will experience a temperature higher than 41.6 °C. According to the transient temperature model, the maximum temperature is 92.0 °C. Likewise, the cold case in Section 3.2 predicted a temperature far lower than that predicted by the transient temperature model. While the steady state case predicted a minimum temperature of -98.9 °C, the minimum transient temperature is -24.3 °C.

Despite the discrepancy in maximum and minimum temperatures between the steady state and transient temperature models, there is some validity in the transient model. This can be seen when Figures 4 and 20 are compared. Both figures follow the same general trend. Although the changes in temperature in Figure 20 are more dramatic than Figure 4, both figures show a slow decrease in temperature as the satellite orbits away from the Sun, and then a rapid

37

decrease as the Earth eclipses the satellite. Both figures then show that a rapid temperature increase as the satellite orbits out of eclipse. While the analysis performed here requires further refinement, the fact that Figure 20 shows the same trend as Figure 4 indicates that the analysis is on a sound path.

If the same transient analysis is performed for the same thermal coatings used in Section 3.3, a similar pattern as Figure 20 is observed (see Figure 21). For each thermal coating, the initial temperature was the hot case temperature calculated in Section 3.3 for that specific coating. $dT/d\phi$ was calculated in MATLAB, and a new temperature was determined for every 3.75° along the CubeSat's orbit. Figure 22 shows the mean temperature of the CubeSat of all seven thermal coatings that were analyzed including the case involving no thermal coating, while the vertical bars indicate how far the temperatures of all eight cases deviate from the mean at that particular point along the orbit. Table 8 shows the maximum and minimum temperatures for each curve in Figure 21, and Table 9 shows the mean temperatures for select points along the curve in Figure 22.
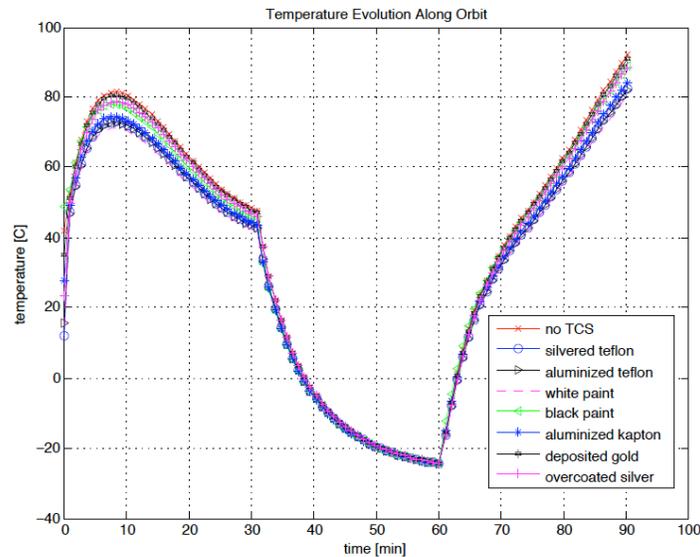
Figure 21: Time evolution of CubeSat temperature with various thermal coatings.

38
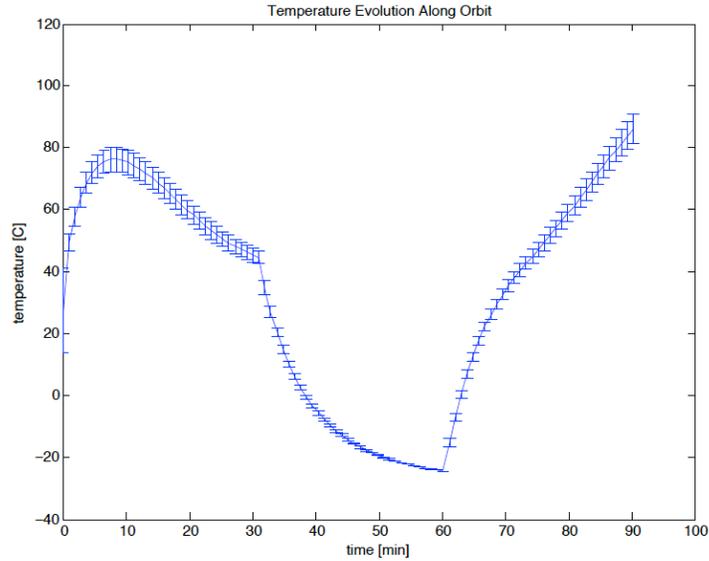
Figure 22: Mean CubeSat temperature with thermal coatings.

Table 8: Maximum and Minimum Temperatures for Thermal Coatings

Surface Coating	Initial Temperature [°C]	Max Temperature [°C]	Min. Temperature [°C]
Optical Solar Reflector			
2-mil silvered Teflon	12.0	82.2	-24.4
2-mil aluminized Teflon	15.3	82.0	-24.4
White Paint			
PCBZ	14.5	80.2	-24.4
Black Paint			
3M Black Velvet	48.8	88.8	-24.4
Aluminized Kapton			
2 mil	27.5	84.1	-24.4
Metallic			
Vapor-deposited gold	35.0	90.7	-24.3
FSS-99 (overcoated silver)	23.2	88.6	-24.3
No coating	41.6	92.0	-24.3
Ave. Temperatures (°C)	27.4	86.1	-24.4

Table 9: Mean Temperature for Select Times Along CubeSat Orbit

Time [sec]	0	10	20	30	40	50	60	70	80	90
Temp. [°C]	27.4	75.2	58.0	45.3	-5.8	-20.0	-24.4	35.4	61.2	86.1

The temperature curves in Figure 21 and 22 and the data presented in Tables 8 and 9 converge to a minimum temperature of -24.4 °C at approximately 60 seconds into an orbit. At 60 seconds the CubeSat is about to transit out of eclipse and into direct sunlight. This suggests that the coldest temperature the CubeSat will reach while in eclipse is -24.4 °C. When compared to the operational and survival temperature ranges in Table 4, -24.4 °C is slightly outside of those ranges. Therefore, thermal coating alone will not be enough to keep the internal components of the CubeSat sufficiently warm while in eclipse.

The hottest temperature the CubeSat may reach varies with the thermal coating, but the mean temperature is approximately 86.1 °C. When this is compared to the temperature ranges in Table 4, 86.1 °C is outside the ranges the internal instruments can operate and survive. Therefore, while the thermal coatings analyzed here may be marginally close to keeping the internal instruments warm enough to operate and survive in eclipse, they do not provide enough coverage to keep the instruments cool enough to operate or survive in direct sunlight.

5.0 Conclusion and Future Work

The transient temperature analysis indicated that the CubeSat will have at its coldest a temperature of -24.4 °C, which is outside the operational and survival temperature ranges for typical spacecraft components. However, this analysis did not take into account the heat generated by the internal components. Therefore, it is possible the internal heat could increase the temperature of the CubeSat such that it will fall within the required operational and survival temperature ranges.

While taking into account internal heat can be favorable when the CubeSat is in eclipse, it can be unfavorable when the CubeSat is in direct sunlight. The transient temperature analysis

showed the CubeSat would be too hot while in direct sunlight. Adding internal heat will only increase the temperature of the satellite further. Therefore, the TCS must be refined.

One positive can be taken away from this analysis, and that is the CubeSat could be sufficiently warm in eclipse solely from the heat generated by the Earth's infrared radiation and the internal instruments of the spacecraft, since Earth's infrared is the only form of radiation present during eclipse. Therefore, an ideal TCS could consist of an external covering for the CubeSat – whether it be a thermal coating, MLI blanket, or a combination of both – that reflects visible light – sunlight and Earth's albedo – but absorbs Earth's infrared radiation. Such TCS will need to be investigated further analytically and through computer simulations, using programs such as Thermo Desktop. Lastly, thermal testing on actual instruments must be performed to validate both analytical and computer models.

References

[1]"Coronal Mass Ejections." *Space Weather Prediction Center*. National Oceanic and Atmospheric Administration, n.d. Web. 30 Jan. 2015.
<http://www.swpc.noaa.gov/phenomena/coronal-mass-ejections>

[2]"Coronal Mass Ejections." *Coronal Weather Report*. n.p., n.d. Web. 30 Jan. 2015.
<http://cse.ssl.berkeley.edu/coronalweather/CMEsFlares/page3.html>

[3]"Geomagnetic Storms." Space Weather Prediction Center. National Oceanic and Atmospheric Administration, n.d. Web. 1 Feb 2015. < http://www.swpc.noaa.gov/phenomena/geomagnetic-storms>

[4]Chenette, D. "Heliophysics." National Aeronautics and Space Administration. 9 Apr. 2014.

[5]Brown, C.D. *Elements of Spacecraft Design*. Reston, VA: American Institute of Aeronautics and Astronautics, 2002.

[6]Wertz, J.R. *Space Mission Analysis and Design*. El Segundo, CA: Microcosm Press, 1999. Print.

[7]Hansen, F. "DTU Satellite Systems Design Course: Cubesat Thermal Design." Danish Space Research Institute. 29 Aug. 2001 Lecture.
<http://www.space.aau.dk/cubesat/documents/Cubesat_Thermal_Design.pdf>

[8]Karam, R.D. *Satellite Thermal Control for Systems Engineers*. Reston, Va: American Institute of Aeronautics and Astronautics, 1998. Print.

[9]Gilmore, D.G., ed. *Spacecraft Thermal Control Handbook*. Vol. 1. El Segundo, CA: Aerospace Press, 2002. Print.

[10]Finckenor, M.M., Dooling, D., *Multilayer Insulation Material Guidelines*. MSFC, Al: Marshall Flight Center, 1999. Print.

[11]Mission Design Division Staff. *Small Spacecraft Technology State of the Art*. Moffett Field, CA: NASA Ames Research Center, 2014. Print.

[12]Mai, T. "Technology Readiness Level" *NASA*, 30 July 2015. Web. 3 Sept. 2015.
<https://www.nasa.gov/directorates/heo/scan/engineering/technology/txt_accordion1.html>

[13]"Environmental Control and Life-support Subsystem (ECLSS)". Federal Aviation Administration. Web. 1 June 2015.
<https://www.faa.gov/other_visit/aviation_industry/designees_delegations/designee_types/ame/media/Section%20III.4.4.1%20Environmental%20Control%20and%20life%20support.pdf>

[14]Vlassov, V.V., Sousa, F.L.de, Cuco, A.P.C., Silva Neto, A.J., "New Concept of Space Radiator with Variable Emittance." *Journal of the Brazilian Society of Mechanical Sciences and Engineering* 32.4 (2010): 400-408. Print.

[15]Tirro, S. *Satellite Communication System Design*. New York: Springer Science and Business Media, 1993. Print.

[16]Shin, K.B., Kim, C.G., Hong, C.S., Lee, H.H. "Thermal Distortion Analysis of Orbiting Solar Array Including Degradation Effects of Composite Materials." *Composites Part B: Engineering* 32.4 (2001): 271-285. Print.

[17]Narayana, K.B., Reddy, V.V. "Thermal Design and Performance of HAMSAT." Acta Astronautcia 60.1 (2007): 7-16. Print.

[18]Woods, T. *Miniature X-ray Solar Spectrometer (MinXSS) CubeSat Mission.* Boulder, CO: 2013. Print.

[19]Kramer, H. "TechEdSat-4 (Technological and Educational Nanosatellite-4)." *eoPortal Directory*. n.d. Web. 20 March 2015. < https://directory.eoportal.org/web/eoportal/satellite-missions/content/-/article/techedsat-4>

[20]Carlisle, C. "Space Technology 5 – A Successful Micro-Satellite Constellation Mission." *21st Annual AIAA/USU Conference on Small Satellites*. n.d. Print.

[21]Price, M. "PH 508: Spacecraft Systems – Thermal Balance and Control." University of Kent. 2011. Lecture.

[22]Martinez, I., "Heat Transfer and Thermal Radiation Modeling." Technical University of Madrid. Lecture. < http://webserver.dmt.upm.es/~isidoro/>

[23]Martinez, I., "Spacecraft Thermal Modelling and Testing." Technical University of Madrid. Lecture.

[24]*29.5% NeXt Triple Junction (XTJ) Solar Cells*. Sylmar: Spectrolab, inc. 2010. Print.

[25]Campbel, W. "Earth-sized Sphere with Topography." MATLAB Central File Exchange, 30 March 2010. Web. 15 Sept 2015. <http://www.mathworks.com/matlabcentral/fileexchange/27123-earth-sized-sphere-with-topography/content/earth_sphere.m>

[26]Condoleo, E. "Orbit3D." MATLAB Central File Exchange, 18 Feb 2014. Web. 15 Sept 2015. <http://www.mathworks.com/matlabcentral/fileexchange/45573-orbit3d/content/Orbit3D/Orbit3D.m>

Appendix A: MATLAB Code for Orbit Plots

The following MATLAB code was used to plot Figure 11. It combines "earth_sphere" code

written by Will Campbell and "Orbit3D" code written by Ennio Condoleo[25,26].

```matlab
%% Plots of Orbits with Different Beta Angles

% An orbit's beta angle is the angle between the orbital plane and solar
% vector.  For all intents and purposes of this exercise, it is assumed
% that the inclination angle of the orbit is equal to the orbit's beta
% angle.

clear all
close all
clc
RE = 6378;            % Earth's radius                        [km]
muE = 398600.44;      % Earth gravitational parameter         [km^3/sec^2]
wE = (2*pi/86164);    % Earth rotation velocity aorund z-axis [rad/sec]


% orbit input
RAAN    = 290.4;              % Right ascension of ascending node [deg]
w       = 331.3;              % argument of perigee [deg]
v0      = 189.8;              % true anomaly [deg]
i       = [0 -30 -60 -90];    % inclination [deg]
a       = 6784.5;             % semi-major axis [km]

% Negative inclination angles were used for plotting purposes only.
% Negative inclination angles were used so that the Sun can be said to be
% facing the y-z plane with solar vectors penetrating y-z plane.  In
% reality, inclination angles would be positive.


% maximum value of eccentricity allowed
ecc_max = sprintf('%6.4f',1-RE/a);
e       = 0.0005;            % eccentricity

% convert to radians
RAAN  = RAAN*pi/180;         % RAAN                         [rad]
w     = w*pi/180;            % Argument of perigee          [rad]
v0    = v0*pi/180;           % True anomaly at the departure [rad]
i     = i*pi/180;            % inclination                  [rad]

% orbit computations
rp = a*(1-e);                % radius of perigee            [km]
ra = a*(1+e);                % radius of apogee             [km]
Vp = sqrt(muE*(2/rp-1/a));   % velocity at the perigee      [km/s]
Va = sqrt(muE*(2/ra-1/a));   % velocity at the  apogee      [km/s]
n  = sqrt(muE./a^3);         % mean motion                  [rad/s]
p  = a*(1-e^2);              % semi-latus rectus            [km]
T  = 2*pi/n;                 % period                       [s]
h  = sqrt(p*muE);            % moment of the momentum       [km^2/s]
```

```matlab
for j = 1:4
    h1(j) = sin(i(j))*sin(RAAN);        % x-component of unit vector h
    h2(j) = -sin(i(j))*cos(RAAN);       % y-component of unit vector h
    h3(j) = cos(i(j));                  % z-component of unit vector h
    n1(j) = -h2(j)/(sqrt(h1(j)^2+h2(j)^2)); % x-component of nodes' line
    n2(j) =  h1(j)/(sqrt(h1(j)^2+h2(j)^2)); % y-component of nodes' line
    n3(j) = 0;                          % z-component of nodes' line
    N(:,j)  = [n1(j),n2(j),n3(j)];           % nodes' line (unit vector)
end

% PRINT SOME DATA
hours   = floor(T/3600);                    % hours   of the orbital period
minutes = floor((T-hours*3600)/60);         % minutes of the orbital period
seconds = floor(T-hours*3600-minutes*60);   % seconds of the orbital period
fprintf('\n Radius of perigee [%10.3f km]      Altitude of perigee [%10.3f
km]',rp,rp-RE);
fprintf('\n Radius of  apogee [%10.3f km]      Altitude of  apogee [%10.3f
km]',ra,ra-RE);
fprintf('\n Velocity at the perigee [%6.4f km/s]   Velocity at the apogee
[%6.4f km/s]',Vp,Va);
fprintf('\n Orbital Period    [%3d h: %3d m: %3d s] ',hours,minutes,seconds);
fprintf('   = [%10.2f s]\n',T);

% TIME
norb = 1;  % number of orbits
t0   = 0;                                    % initial time          [s]
tf   = norb*T;                               % final   time          [s]
step = 120;                                  % time step             [s]
t    = t0:step:tf+step;                       % vector of time        [s]


% DETERMINATION OF THE DYNAMICS

% cosine of initial eccentric anomaly
cosE0 = (e+cos(v0))./(1+e.*cos(v0));

% sine of initial eccentric anomaly
sinE0 = (sqrt(1-e^2).*sin(v0))./(1+e.*cos(v0));

% initial eccentric anomaly [rad]
E0 = atan2(sinE0,cosE0);
if (E0<0)                                % E0[0,2pi]
    E0=E0+2*pi;
end
tp = (-E0+e.*sin(E0))./n+t0;              % pass time at the perigee   [s]
M  = n.*(t-tp);                           % mean anomaly

% Mk = Ek - e*sin(Ek);
% Eccentric anomaly (must be solved iteratively for Ek)
E = zeros(size(t,2),1);
for j=1:size(t,2)
    E(j) = anom_ecc(M(j),e);             % eccentric anomaly         [rad]
end

% True anomaly, Argument of latitude, Radius
sin_v = (sqrt(1-e.^2).*sin(E))./(1-e.*cos(E));  % sine of true anomaly
cos_v = (cos(E)-e)./(1-e.*cos(E));              % cosine of true anomaly
```

```matlab
v     = atan2(sin_v,cos_v);               % true anomaly [rad]
theta = v + w;                            % argument of latitude [rad]
r     = (a.*(1-e.^2))./(1+e.*cos(v));     % radius [km]

% Satellite coordinates
% "Inertial" reference system ECI (Earth Centered Inertial)
xp = r.*cos(theta); % In-plane x position (node direction)          [km]
yp = r.*sin(theta); % In-plane y position (perpendicular node direct.) [km]

for j = 1:4
    xs(:,j) = xp.*cos(RAAN)-yp.*cos(i(j)).*sin(RAAN); % ECI x-coord. SAT [km]
    ys(:,j) = xp.*sin(RAAN)+yp.*cos(i(j)).*cos(RAAN); % ECI y-coord. SAT [km]
    zs(:,j) = yp.*sin(i(j));                          % ECI z-coord. SAT [km]

end

rs = p./(1+e.*cos(theta-w));              % norm of radius SAT

% Determine eclipse time

alt = a - RE;
i = i*180/pi;


% eclipse fraction of a circular orbit
for j = 1:4
        fE(j,1) = (1/180)*acosd(((alt^2+2*RE*alt)^0.5)...
            /(a*cosd(i(j))));
end

% Total time of eclipse in [sec]
Te = T*fE;

fprintf('\n 0 deg inclination = 2165 sec in eclipse');
fprintf('\n 30 deg inclination = 2064 sec in eclipse');
fprintf('\n 60 deg inclination = 1452 sec in eclipse');
fprintf('\n 90 deg inclination = 0 sec in eclipse \n');

% This corresponds to 19 indices of the time vector, t, for 0 deg
% inclination, 18 indices of the time vector for 30 deg inclination, 13
% indices for 60 deg inclination and 0 for 90 deg inclination.  This means
% there are those number of indices in the position coordinates, xs, ys,
% and zs, that are in eclipse (ie 19 xs, ys, and zs for 0 deg inclination
% in eclipse, 18 xs, ys, and zs for 30 deg inclination, etc.)

%% Plot orbits

% If sun is assumed to be facing y-z plane and sunlight is penetrating y-z
% plane, then the midpoint of eclipse is behind Earth at ys = 0.  Now,
% divide the number of indices in eclipse by half.  From there, plot half
% of those indices at ys>0 and ys<0 to show total time in eclipse.


figure(1),
subplot(221),
```

```matlab
earth_sphere,
hold on, plot3(xs(1:2,1),ys(1:2,1),zs(1:2,1),'r->','linewidth',2)
hold on, plot3(xs(3:22,1),ys(3:22,1),zs(3:22,1),'k->','linewidth',2)
hold on, plot3(xs(23:48,1),ys(23:48,1),zs(23:48,1),'r->','linewidth',2)
title('\beta  angle = 0 [deg]')

subplot(222),
earth_sphere,
hold on, plot3(xs(1:4,2),ys(1:4,2),zs(1:4,2),'r->','linewidth',2)
hold on, plot3(xs(5:23,2),ys(5:23,2),zs(5:23,2),'k->','linewidth',2)
hold on, plot3(xs(24:48,2),ys(24:48,2),zs(24:48,2),'r->','linewidth',2)
title('\beta  angle = 30 [deg]')

subplot(223),
earth_sphere,
hold on, plot3(xs(1:6,3),ys(1:6,3),zs(1:6,3),'r->','linewidth',2)
hold on, plot3(xs(7:19,3),ys(7:19,3),zs(7:19,3),'k->','linewidth',2)
hold on, plot3(xs(20:48,3),ys(20:48,3),zs(20:48,3),'r->','linewidth',2)
title('\beta  angle = 60 [deg]')

subplot(224),
earth_sphere,
hold on, plot3(xs(:,4),ys(:,4),zs(:,4),'r->','linewidth',2)
title('\beta  angle = 90 [deg]')

% Black indicates when spacecraft is in eclipse, red indicates when
% spacecraft is in direct sunlight.
```

Appendix B: Calculations for Steady State Temperature

Hot Case

To determine the temperature of the CubeSat, the energy balance described by Equation (2.2.7) is used. The heat absorbed by the CubeSat is found first. As stated in Section 3.2, solar radiation is incident on one longitudinal face and the two lateral faces at 90° and 45°, respectively. The heat resulting from the solar radiation is found using Equation (2.2.1).

$$Q_S = S(\alpha_{long}A_{long}\cos\theta_{long} + \alpha_{lat}A_{lat}\cos\theta_{lat}) = 37.11 \text{ W} \tag{B.1}$$

where A_{long} = 300 cm², θ_{long} = 90°, A_{lat} = 100 cm², θ_{lat} = 45°, $\alpha_{lat} = \alpha_{al}$ = 0.379, and

$$\alpha_{long} = \frac{\alpha_s A_s + \alpha_{al}A_{al}}{A_{long}} = \frac{(0.9)(200 \text{ cm}^2) + (0.379)(100 \text{ cm}^2)}{300 \text{ cm}^2} = 0.726 \tag{B.2}$$

The composition of the longitudinal face is a combination of solar cells and aluminum. The solar cells make up an area of 200 cm² while the aluminum makes up an area of 100 cm². Therefore, the absorptivity of the longitudinal face is a weighted average of the two materials as calculated in Equation (B.2). The absorptivity of the lateral faces is simply the absorptivity of the aluminum.

The radiation from albedo is incident at 90° on the longitudinal face facing the Earth. The heat resulting from albedo can be calculated from Equation (2.2.2).

$$Q_A = S'\alpha_s A_{long}\cos\theta = 9.60 \text{ W} \tag{B.3}$$

where θ = 90°, and

$$S' = (\text{albedo})(S) = (0.26)(1367 \text{ W/m}^2) = 355 \text{ W/m}^2 \tag{B.4}$$

Similar to the radiation from albedo, Earth's infrared radiation is incident on the side facing the Earth at 90°. The heat from infrared radiation is found using Equation (2.2.4).

$$Q_E = A_{long}\epsilon_s F_{12}S_E = 5.80 \text{ W} \tag{B.5}$$

where $F_{12} = 0.8853$.

The total heat absorbed from the environment is

$$Q_a = Q_S + Q_A + Q_E = 52.5 \text{ W} \tag{B.6}$$

The temperature of the CubeSat is found using the energy balance of Equation (2.2.7).

$$Q_a = Q_e \tag{B.7}$$

where

$$Q_e = (\epsilon' A_{long} + 3(\epsilon_s A_{long}) + 2(\epsilon_{al} A_{lat}))\sigma T^4 \tag{B.8}$$

$$\epsilon' = \frac{\epsilon_s A_s + \epsilon_{al} A_{al}}{A_{long}} = \frac{(0.85)(200 \text{ cm}^2) + (0.0393)(100 \text{ cm}^2)}{300 \text{ cm}^2} = 0.5798 \tag{B.9}$$

and $\sigma = 5.66 \times 10^{-8}$ W/m²K⁴.

Unlike the absorbed radiation, the radiation emitted by the CubeSat is emitted from all six sides of the CubeSat, hence Equation (B.8). Like the weighted absorptivity, the longitudinal side that consists of both solar cells and aluminum has a weighted emissivity. The other three longitudinal sides consist solely of solar cells, and the two lateral faces consist of aluminum. Thus, the temperature of the CubeSat for the hot case is

$$T = \left(\frac{Q_a}{(\epsilon' A_{long} + 3(\epsilon_s A_{long}) + 2(\epsilon_{al} A_{lat}))\sigma}\right)^{\frac{1}{4}} - 273 \text{ K} = 41.6 \text{ °C} \tag{B.10}$$

Cold Case

The calculations for the CubeSat temperature for the cold case followed the same steps as that for the hot case. The main difference is that the solar radiation and albedo are zero. The albedo is zero because there is no reflected solar radiation when the CubeSat is in eclipse. The only radiation the CubeSat is exposed to and absorbs is Earth's infrared.

$$Q_E = A_{long} \epsilon_s F_{12} S_E = 4.92 \text{ W} \tag{B.11}$$

$$Q_a = Q_S + Q_A + Q_E = 0 + 0 + 4.92 \text{ W} = 4.92 \text{ W} \tag{B.12}$$

Equations (2.2.7) and (B.8) are again used to determine the temperature of the CubeSat

for the cold case.

$$T = \left(\frac{Q_a}{\left(\epsilon' A_{long} + 3\left(\epsilon_s A_{long} \right) + 2\left(\epsilon_{al} A_{lat} \right) \right) \sigma} \right)^{\frac{1}{4}} - 273 \text{ K} = -98.9 \text{ °C} \tag{B.13}$$

Appendix C: Transient Temperature MATLAB Code

```matlab
%% Transient temperature of Helios CubeSat

clc, clear all

% Define known parameters
i = 51.6;               % inclination [deg]
H = 400;                % altitude [km]
R = 6370;               % Earth radius [km]
abs = 0.7263;           % weighted absorptivity of spacecraft
A = 0.14;               % total area of spacecraft [m^2]
Af = 0.03;              % frontal area [m^2]
Es = 1370;              % solar irradiance [W]
alb = 0.26;             % albedo
m = 3;                  % mass of spacecraft[kg]
cp = 896;               % heat capacity of Al 6061-t6 [J/kg.K]
Tp = 288;               % temperature of planet [K]
eb = 0.5798;            % weighted emissivity of spacecraft
sig = 5.67e-8;          % Stefan-Boltzmann constant
ep = 0.6;               % emissivity of planet
P = 5420;               % period of orbit [s]
Fb0 = 1;                % view factor of unity
Fbp = 0.8853;           % view factor
T = 314.6;              % initial temperature [K]


h = (H+R)/R;            % function of relative orbit radius


beta = i*pi/180;     % beta angle [rad]
beta_max = pi/2 - acos(1/h);


% Define heat fluxes
Qs0 = abs*Af*Es;                % solar input
Qa0 = abs*A*Fbp*alb*Es;         % abledo input
Qp = eb*A*Fbp*ep*sig*Tp^4;      % infrared input


% Define orbital angle range and intervals
phi = 0:pi/48:2*pi;



% angular position eclipse starts
phi_s = pi - acos(sqrt(h^2 - 1)/(h*cos(beta)));      % [rad]



% angular position eclipse ends
phi_e = pi + acos(sqrt(h^2 - 1)/(h*cos(beta)));      % [rad]

% step function for solar input
for i = 1:97
    if phi_s < phi(i) && phi_e > phi(i)
        Fs(i) = 0;
    else
        Fs(i) = 1;
    end
end
```

```matlab
% albedo view factor from 0 to 180 deg
for i = 1:49
    if phi(i) > phi_s && phi(i) < pi
        Fe(i) = 0;
    else
        Fe(i) = 1;
    end
    Fa(i) = (0.5+0.5*cos(phi(i)))^2*(1-(phi(i)/phi_s)^2)*Fe(i);

end

%albedo view factor from 180 to 360 deg
for i = 50:97
    if phi(i) < phi_e && phi(i) > pi
        Fe(i) = 0;
    else
        Fe(i) = 1;
    end
     Fa(i) = -(0.5+0.5*cos(phi(i)))^2*(1-(phi(i)/phi_e)^2)*Fe(i);
end

Qs = Qs0*Fs;
Qa = Qa0*Fa;
Qp = 0*phi + Qp;

% initial temperature.  Taken from hot case calculations
T = 314.6;

% Determine change in temperature for each change in angle.  Add that
% change to previous temperature to obtain new temperature.  Repeat
% process.
for i = 1:96
    dT_dphi(i) = (P/(m*cp*2*pi))*(Qs0*Fs(i) + Qa0*Fa(i) + Qp(i) ...
        - eb*A*Fb0*sig*T(i)^4);
    T(i+1) = T(i) + dT_dphi(i);
end

dT_dphi(97) = (P/(m*cp*2*pi))*(Qs0*Fs(97) + Qa0*Fa(97) + Qp(97) ...
    - eb*A*Fb0*sig*T(97)^4);

% convert from [rad] to [deg]
phi_s = phi_s*180/pi;                                    % [deg]
phi_e = phi_e*180/pi;                                    % [deg]
phi = phi*180/pi;


% Plot solar input
figure(1),
plot(phi,Qs,'linewidth',2)
axis([0 360 0 40]),
title('Solar Heat Flux Along Orbit'),
xlabel('Orbital Angle, \phi [deg]'), ylabel('Solar Heat Flux [W]')

% Plot albedo input
figure(2),
plot(phi,Qa,'linewidth',2)
```

```matlab
title('Albedo Heat Flux Along Orbit'),
xlabel('Orbital Angle, \phi [deg]'), ylabel('Albedo Heat Flux [W]')

% Convert angle to time
t = phi*P/(360*60);

T = T - 273;        % convert from Kelvin to Celsius

% Plot time evolution of temperature
figure(3),
plot(t,T,'linewidth',2), grid on
xlabel('time [min]'), ylabel('temperature [C]')
title('Temperature Evolution Along Orbit')
```